applied optics

Removal of all mosaic grating errors in a single-interferometer system by a phase-difference reference window

Yuxian Lu,[1,2] Xiangdong Qi,[1] Xiaotian Li,[1] Haili Yu,[1,*] Shan Jiang,[1] Heshig Bayan,[1] and Lu Yin[1,2]

[1]Grating Technology Laboratory, Changchun Institute of Optics and Fine Mechanics and Physics, Chinese Academy of Sciences, Changchun, Jilin 130033, China
[2]University of Chinese Academy of Sciences, Beijing 100049, China
*Corresponding author: yuhailitc@163.com

Received 13 May 2016; revised 22 July 2016; accepted 10 August 2016; posted 11 August 2016 (Doc. ID 265116); published 28 September 2016

An interference method to remove all mosaic grating errors using a phase-difference reference window without compensation for coupled mosaic errors or analyzing the far-field diffraction intensity patterns is proposed. The reference window is achieved by adding a small-aperture prism; therefore, the incident light on the mosaic gratings contains two different angles of incidence and optical paths, eliminating the uncertainty of longitudinal mosaic error in the interferometer. The mathematical model of the method is established and optical arrangement is presented. Interference fringes with the reference window and alignment process are simulated and the accuracy of mosaic errors are analyzed. The experimental and simulation results show that our method can eliminate longitudinal mosaic error and all other mosaic grating errors. The accuracy of angle mosaic errors can be less than 1 μrad and position mosaic errors can be to the nanometer level. Compared with the far-field diffraction intensity patterns method, our method reduces the complexity of the optical structure and ensures measurement accuracy. © 2016 Optical Society of America

OCIS codes: (050.0050) Diffraction and gratings; (120.0120) Instrumentation, measurement, and metrology; (120.4640) Optical instruments.

http://dx.doi.org/10.1364/AO.55.007997

1. INTRODUCTION

Large-aperture diffraction gratings are important optical elements in many fields, such as the astronomical telescope field to improve spectral resolution [1–5], and the petawatt chirped-pulse laser field to increase laser damage thresholds [6–9], among others [10,11]. With the increase in grating size requirements, it is technically impractical to manufacture monolithic gratings. An effective way is to mosaic two or more gratings [12,13] which are made by current technologies to form an equivalent single large-size grating. However, the accuracy requirements in alignment of the positions and orientations of the constituent gratings are extremely high [14,15]. If the mosaic gratings are required to be used at any wavelength or angle of incidence [15], the following conditions must be satisfied: the constituent gratings' surfaces must be coplanar; the constituent gratings' grooves must be parallel; and the gap between constituent gratings is an integer multiple of the grating period.

For the "perfect mosaic," which is satisfied with the above conditions, the alignment process is even harder. High-accuracy measurement is very important during the alignment process. Five degrees of freedom affect the alignment accuracy of mosaic gratings. For a perfect mosaic, it is significant to separate and eliminate each degree of freedom in the process of adjustment. There are two methods to measure mosaic errors, including analyzing the interference fringes [16,17] and analyzing the far-field diffraction intensity patterns [18,19]. Qiao *et al.* adopted real-time interferometer tiling control and reconstructed the overall wavefront on diffraction order. This is a compensative mosaic method in which coupled mosaic errors compensate with each other to achieve minimum diffraction wave front error, with limitations of the specific wavelength and angle of incidence [20]. Zeng and Li proposed a two-color heterodyne interferometer to separate and eliminate the lateral and longitudinal phase errors using two wavelengths, but detection of the angular errors was not mentioned [15]. Hu and Zeng have demonstrated the far-field energy measurement to measure the zero-order and first-order far-field patterns at two wavelengths to realize a perfect mosaic [18]. Another study employed the interferometer and far-field diffraction intensity patterns at two wavelengths at the same time, because the longitudinal error cannot be eliminated on the zero order in an interferometer system; therefore, it is essential to analyze

far-field energy at two wavelengths to separate and eliminate the longitudinal and lateral mosaic errors [19]. The input wavefront error is the dominant factor that determines the interference fringes' and the far-field diffraction intensity patterns' quality [20]. Because the optical path for the far-field diffraction intensity patterns method is more complex than the interference method, it is more difficult for the far-field diffraction intensity patterns method to reduce input wavefront error, resulting in the decrease of measuring accuracy of the mosaic errors. Therefore, it is essential to remove mosaic grating errors without introducing far-field diffraction intensity patterns to realize a perfect mosaic.

In this paper, we propose an optical path with a single-interferometer system to eliminate five-dimensional mosaic errors. This is achieved by adding a small-aperture prism in the interferometer to produce different phase differences. The non-coplanar mosaic errors are eliminated on the zero order with the help of a small-aperture reference window. The coplanar mosaic errors are eliminated on the first order without the influence of longitudinal error. In Section 2, the relationship between mosaic errors and interference fringes is established, the phase difference between original beam and reference beam is analyzed, and the optical path to realize one beam forming an optical path difference reference window is designed. In Section 3, the interference fringes with a reference window and the alignment process are simulated, and the accuracy of mosaic errors is calculated.

2. MATHEMATICAL MODEL

The coordinates and definitions of the mosaic grating errors are presented in Fig. 1. The surface of grating G_1 is taken as the x–y plane and the z axis is perpendicular to the surface of grating G_1; the x axis is the grating vector and the y axis is the direction of the grating grooves. The mosaic errors between grating G_1 and grating G_2 are as follows: tilt $\Delta\theta_x$, which is rotated around the x axis; tip $\Delta\theta_y$, which is rotated around the y axis; in-plane rotation $\Delta\theta_z$, which is rotated around the z axis; lateral gap Δx, which is moved along the x axis; and longitudinal distance Δz, which is moved along the z axis. In the direction of the right-hand helix, the angle mosaic errors $\Delta\theta_x$, $\Delta\theta_y$, $\Delta\theta_z$ are positive; Δx is always positive and Δz is positive if the surface of grating G_2 is located in a place where z is greater than 0.

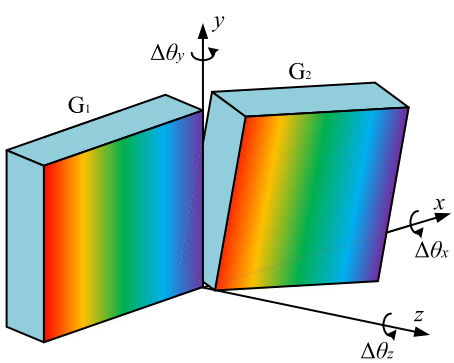

Fig. 1. Definitions of the mosaic grating errors.

Assuming that the grating surface is ideal, the optical path difference (OPD) between G_1 and G_2 can be derived as follows:

$$\Delta(m) = H(\cos\alpha_m + \cos\beta_m) + W\frac{m\lambda}{d}. \tag{1}$$

In Eq. (1), m is the diffraction order, λ is the wavelength of incident light, d is the grating period, α_m is the angle of incidence, and β_m is the angle of diffraction. H is the function of non-coplanar mosaic errors which are caused by $\Delta\theta_x$, $\Delta\theta_y$, and Δz, and W is the function of coplanar errors which are caused by $\Delta\theta_z$ and Δx. If the coordinate of any point on the surface of grating G_2 is (x_i, y_i), then Eq. (1) can be written as

$$\Delta_i(m) = (-y_i\Delta\theta_x + x_i\Delta\theta_y + \Delta z)(\cos\alpha_m + \cos\beta_m) + (y_i\Delta\theta_z + \Delta x)\frac{m\lambda}{d}. \tag{2}$$

The requirements are satisfied for a "perfect mosaic" only if $\Delta_i(m) = k\lambda(k = 0, \pm 1, \pm 2, \ldots)$, which means that: $\Delta\theta_x = 0$, $\Delta\theta_y = 0$, $\Delta\theta_z = 0$, $\Delta x = kd/m$, and $\Delta z = 0$. In an interferometer system, we cannot get OPD directly but instead the interference fringe intensity; the relationship between OPD and interference fringe intensity is:

$$I(x_i, y_i) = A\left\{1 + \cos\left[\frac{2\pi}{\lambda}\Delta_i(m)\right]\right\}. \tag{3}$$

In Eq. (3), I is interference fringe intensity and A is a constant. According to Eq. (3), if $\Delta_i(m) = k\lambda + C\lambda(0 \le C \le 1)$, $\Delta_i(m)$ is equivalent to $\Delta_i(m) = C\lambda$. Therefore we cannot calculate the exact value of $\Delta_i(m)$ with $k\lambda$ missing, which is caused by Δz. This is why previous mosaic grating measurements cannot use interferometry only. In order to solve this problem, we propose a novel idea to calculate Δz accurately in a single-interferometer system instead of the introduction of two wavelengths.

Equation (2) shows that all of the mosaic errors affect the optical path between G_1 and G_2 on the m order ($m \neq 0$), however, non-coplanar errors disappear when $m = 0$. So we calculate and adjust the coplanar errors on the zero order first and the coplanar errors on the m order ($m \neq 0$) afterward. When $m = 0$, $\Delta_i(0) = 2\cos\alpha_0\ (-y_i\Delta\theta_x + x_i\Delta\theta_y + \Delta z)$. Assuming that $\Delta\theta_x = 0$ and $\Delta\theta_y = 0$, because it is relatively easy to adjust $\Delta\theta_x$ and $\Delta\theta_y$ to close to zero, the OPD of the zero order is $\Delta_i(0) = 2\cos\alpha_0\Delta z$. No matter whether $\Delta_i(0) = k\lambda + C\lambda$ or $\Delta_i(0) = C\lambda$, the longitudinal distance Δz measured in interferometer system is $C\lambda/(2\cos\alpha_0)$, with the lack of $k\lambda/(2\cos\alpha_0)$. We adopt two angles of incidence α_{01} and α_{02} to eliminate the uncertainty of Δz; it is based on the different OPD between G_1 and G_2, which is caused by different angles of incidence, as is shown in Fig. 2.

The optical path difference of angle of incidence α_{01} is $\overline{CP} + \overline{PA} = 2\cos\alpha_{01}\Delta z$, and the optical path difference of angle of incidence α_{02} is $\overline{CQ} + \overline{QB} = 2\cos\alpha_{02}\Delta z$. If $\overline{CP} + \overline{PA} = \overline{CQ} + \overline{QB} = C\lambda$, then Δz must be satisfied with

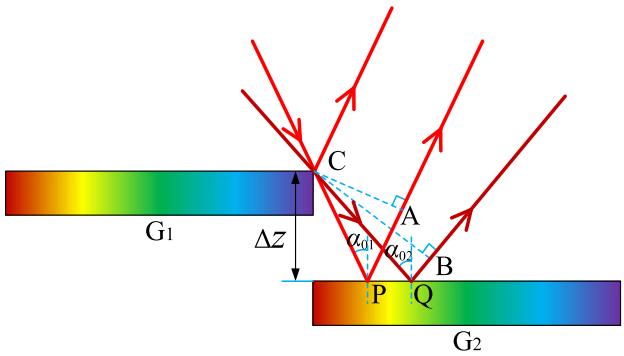

Fig. 2. Optical path difference of two angles of incidence caused by Δz.

$$\Delta z = n f_{\mathrm{lcm}}\left(\frac{C\lambda}{2\cos\alpha_{01}}, \frac{C\lambda}{2\cos\alpha_{02}}\right), \qquad (n = 0, 1, 2, \ldots). \tag{4}$$

In Eq. (4), f_{lcm} is the function of "least common multiple."

For a "perfect mosaic," it requires $\Delta z = 0$, which means the parameter $C = 1$ in Eq. (4). Except for $\Delta z = 0$, the minimum value of Δz is $\Delta z_{\min} = f_{\mathrm{lcm}}[\lambda/(2\cos\alpha_{01}), \lambda/(2\cos\alpha_{02})]$. When $\Delta z = \Delta z_{\min}$, there is no interference fringe dislocation for the two angles of incidence α_{01} and α_{02} for the first time (except for $\Delta z = 0$). When $\Delta z = n \cdot \Delta z_{\min}$, there is no interference fringe dislocation for the two angles of incidence α_{01} and α_{02} for the nth time (except for $\Delta z = 0$). If $\Delta z_{\min}$ is distinguished by the eyes, the uncertainty of Δz can be eliminated easily. When the initial value of Δz is less than $\Delta z_{\min}$, during the alignment process, the value of Δz is decreased and the two sets of interference fringes for the two angles of incidence α_{01} and α_{02} have no fringe discontinuities that correspond to $\Delta z = 0$ only.

3. OPTICAL STRUCTURE DESIGN

In order to realize one beam forming two angles of incidence, a small-aperture prism is added to the optical path, which will not affect the OPD between G_1 and G_2. The experimental setup is shown in Fig. 3. The original large-aperture beam without passing through a prism and small-aperture beam passing through a prism form two incident beams, which are reflected by Mirror1 and Mirror2, respectively, forming two sets of interference fringes on the detector. By adjusting the position of Mirror1, the zero-order beam and the m-order ($m \neq 0$) beam can be switched. When the beam is switched to the m order ($m \neq 0$), the prism is moved out.

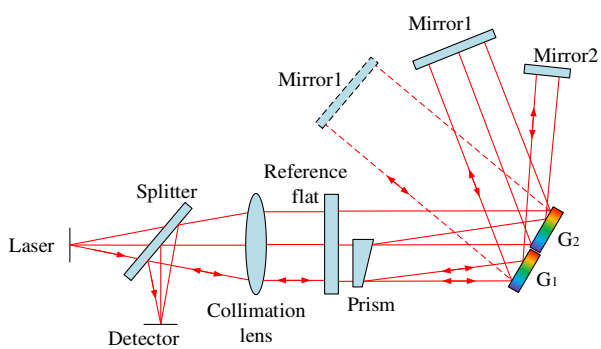

Fig. 3. Design of experimental setup.

The peak intensities of the two different sets of interference fringes obtained for the two different angles of incidence are different because the constant A is different in Eq. (3). Assume that constant A of angle of incidence α_{01} is A_{01}, of angle of incidence α_{02} is A_{02}, and of angle of incidence α_{m1} is A_{m1}, which can be expressed as

$$\begin{cases} A_{01} = D_0^2 R_{M1} \\ A_{02} = T_P^2 D_0^2 R_{M2} \\ A_{m1} = D_m^2 R_{M1} \end{cases}. \tag{5}$$

In Eq. (5), D_0 and D_m are the diffraction efficiencies of the mosaic gratings (the parameters of grating G_1 and grating G_2 are the same) on the zero order and m order, respectively; R_{M1} and R_{M2} are the reflectivity of Mirror1 and Mirror2, respectively; and T_P is the transmission of the prism.

The selection of α_{01} and α_{02} depends on the size and apex angle of the prism, the relative position between the prism and the reference flat, the size of the mosaic gratings and their relative position with the reference flat, and the distance between the prism and the mosaic gratings; these are shown in Fig. 4.

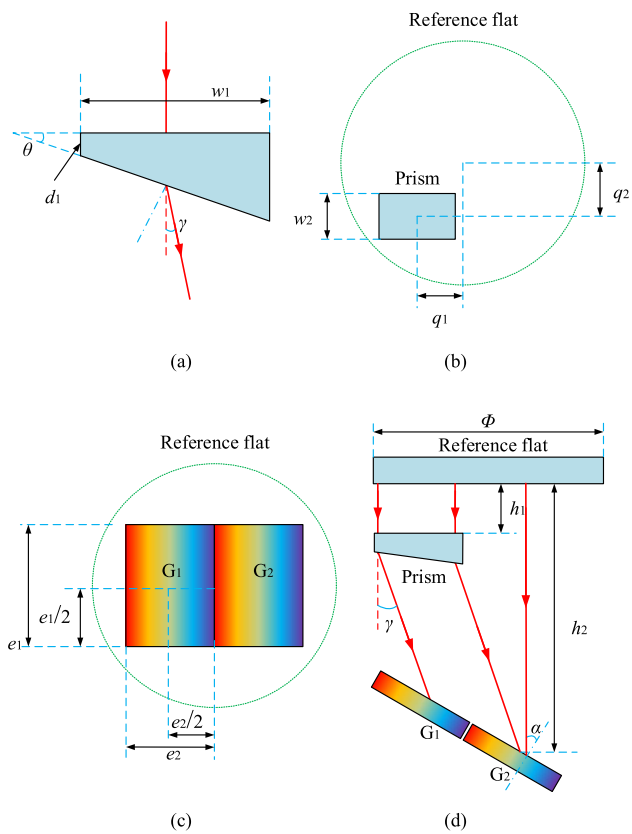

Fig. 4. Parameters design for angles of incidence α_{01} and α_{02}. (a) Size and apex angle of the prism; (b) relative position between the prism and reference flat; (c) size of mosaic gratings and their relative position with reference flat; and (d) distance between the prism and mosaic gratings.

Table 1. Detailed Parameters for Angles of Incidence α_{01} and α_{02}

Parameter	Value
w_1	30 mm
w_2	20 mm
d_1	5 mm
θ	10°
γ	5.0981°
q_1	17 mm
q_2	1 mm
e_1	35 mm
e_2	30.31 mm
Φ	100 mm
α	30°
h_1	100 mm
h_2	440 mm

Because the two angles of incidence are realized by one beam instead of two, the angles α_{01} and α_{02} cannot be very different or the small-aperture beam will deviate from the gap of the mosaic gratings. A distance of greater than 100 μm is easy to be distinguished, so the angles of incidence with $\Delta z_{\min}$ greater than 100 μm can be selected in principle. However, the angles of incidence cannot be too high because the decreased beam width will cause reduced resolution. In light of these considerations, the detailed design parameters are listed in Table 1.

4. EXPERIMENTAL RESULTS AND DISCUSSION

Based on these overall considerations, a large-aperture beam with an angle of incidence $\alpha_{01} = 30°$ and a small-aperture beam with an angle of incidence $\alpha_{02} = 35.0981°$ were chosen. $\Delta z_{\min}$ was calculated to be 140.89 μm, which means if the initial value of Δz is less than 140.89 μm, when the two sets of interference fringes have no fringe discontinuities, it corresponds to $\Delta z = 0$. The initial surface distance 140.89 μm between the two gratings can be distinguished by the eyes. For fine adjustment, Δz can be calculated using the two interference fringes from the two angles of incidence. If $A_{01} = 0.9$, $A_{02} = 0.7$, the simulation result of the two interference fringes on the zero order is shown in Fig. 5.

There are two sets of fringes: large-aperture fringes formed by the angle of incidence 30° and small-aperture fringes formed by the angle of incidence 35.0981°. The set of small-aperture interference fringes which is marked with a red circle in Fig. 5 is the reference window. The reference window is only for Δz adjustment, because when adjusting $\Delta\theta_x$ and $\Delta\theta_y$, the large-aperture fringes have a higher resolution than the reference window. It is obvious that the reference window region masks a portion of large-aperture interference fringes, which will affect the detection resolution of $\Delta\theta_x$ and $\Delta\theta_y$, so the prism has to move out during $\Delta\theta_x$ and $\Delta\theta_y$ adjustment. By detecting the large-aperture interference fringes and the reference window, the uncertainty of Δz can be eliminated. This method greatly simplifies the complexity of the optical structure caused by Δz. The interference intensity of incidence beams α_{01} and α_{02} are shown in Fig. 6; in order to analyze the detailed information, Δz changes from 0 to 0.14089 nm instead of 0 to 0.14089 mm, and it is clear that when the intensity of α_{01} is equal to 1.8, the intensity of α_{02} is not equal to 1.4. This is why the interference fringes have different discontinuity between the beams of α_{01} and α_{02}.

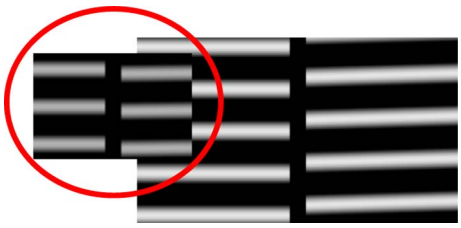

Fig. 5. Simulation result of two interference fringes on the zero order.

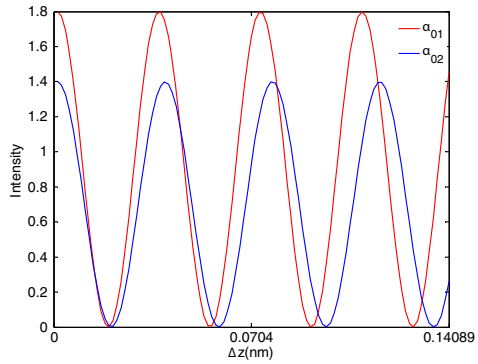

Fig. 6. Simulation result of two interference fringes on the zero order.

After alignment of the non-coplanar errors $\Delta\theta_x$, $\Delta\theta_y$, and Δz on the zero order, the position of Mirror1 is changed to adjust coplanar errors $\Delta\theta_z$ and Δx. Without the influence of $\Delta\theta_x$, $\Delta\theta_y$, and Δz, it is easier to adjust $\Delta\theta_z$ and Δx to be close to zero.

The optical path principle and adjustment steps are as follows in detail:

(1) Optical path principle: a large-aperture beam at an angle of 30° passes mosaic gratings G_1 and G_2 and is reflected by Mirror1, forming large-aperture interference fringes, and according to which, adjusting $\Delta\theta_x$, $\Delta\theta_y$. Then the prism is moved into the optical path, and the large-aperture beam passes through a small-aperture prism, forming a small-aperture beam at an angle of 35.0981°. The beam passes mosaic gratings G_1 and G_2, reflected by Mirror2, to form small-aperture interference fringes.

(2) Detection of the zero-order beam: $\Delta\theta_x$ and $\Delta\theta_y$ are adjusted according to the inclination and width of the large-aperture interference fringes. After the alignment of $\Delta\theta_x$ and $\Delta\theta_y$, the large-aperture interference fringes and small-aperture interference fringes are combined to adjust Δz.

(3) Detection of the diffraction order beam: Mirror1 is moved to change the diffraction order beam. $\Delta\theta_z$ and Δx are adjusted based on the diffraction large-aperture interference fringes.

To verify the correctness of our method, an experimental optical path is set up, which is shown in Fig. 7. The wavelength of the incident beam is 632.8 nm, the grating groove density is 300 gr/mm, and the diffraction is first-order.

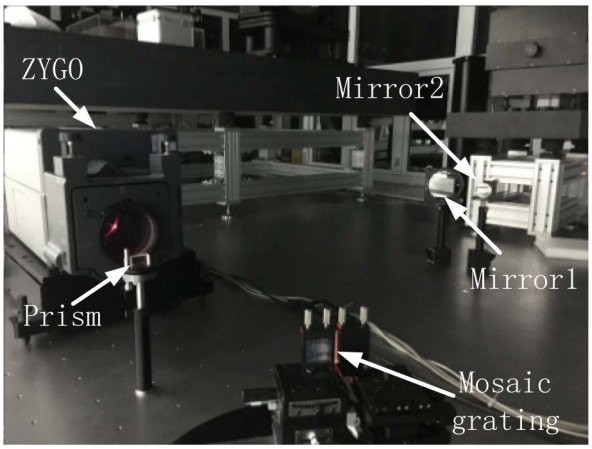

Fig. 7. Experimental optical path.

Figure 8 shows the adjustment process of mosaic errors on the zero order and diffraction order; the left figures are simulated according to the mathematical model, the middle figures are simulated according to ZEMAX, and the right figures are experimental results. The experimental interference is the image by inversion because of the optical structure of ZYGO.

Figures 7(a)–7(f) show the zero-order interference fringes. Figures 7(a) and 7(b) are the process to adjust $\Delta\theta_x$ and $\Delta\theta_y$ to zero. The alignment of $\Delta\theta_x$ changes the width of the fringes, and the alignment of $\Delta\theta_y$ changes the inclination of the fringes. Figures 7(c)–7(f) show that the longitudinal distance Δz changes from 216 nm to −47.633 nm. During this range, the large-aperture fringes and reference window have different discontinuities. Figures 7(g)–7(i) show the first-order interference fringes. The large-aperture fringes are relied on to adjust $\Delta\theta_z$ and Δx. The alignment of $\Delta\theta_z$ affects the width of the fringes, while Δx affects the position of the fringes. It shows the changes of fringes clearly in Fig. 7 during the adjustment of five mosaic errors on the zero order and first order. The results of analysis and experiment are consistent, which verify the correction of the mathematical model and the feasibility of our method.

If the total number of elements of the selected detector is 512×480, and pixel size is $18.512\ \mu\text{m} \times 18.512\ \mu\text{m}$, then for G_1 and G_2 on the detector it is 256×240 and 256×240, respectively. Assuming that the total number pixels of fringes of G_1 is 256×200, if the fringes of G_2 have one pixel offset compared with the fringes of G_1, the OPD is $\lambda/400$. It is obvious that the measured OPD is double that of the OPD between G_1 and G_2. If the lateral axis on the detector is u, the longitudinal axis on the detector is v. According to Eq. (2), the resolutions for mosaic errors are as follows:

$$\begin{cases} 2v_{\max}K\Delta\theta_x \cos\alpha_{01} = \frac{\lambda}{400} \\ 2\frac{u_{\max}K}{\cos\alpha_{01}}\Delta\theta_y \cos\alpha_{01} = \frac{\lambda}{400} \\ 2\Delta z \cos\alpha_{01} = \frac{\lambda}{400} \\ v_{\max}K\Delta\theta_z\frac{m\lambda}{d} = \frac{\lambda}{400} \\ \Delta x\frac{m\lambda}{d} = \frac{\lambda}{400} \end{cases}. \tag{6}$$

In Eq. (5), K is the ratio of the size of object to the size of detector, $u_{\max} = 18.512\ \mu\text{m} \times 256$; $v_{\max} = 18.512\ \mu\text{m} \times 240$; $K = 10$; and the resolution results of mosaic errors are $\Delta\theta_x = 0.020558\ \mu\text{rad}$, $\Delta\theta_y = 0.016691\ \mu\text{rad}$, $\Delta\theta_z = 0.18757\ \mu\text{rad}$, $\Delta x = 8.333$ nm, and $\Delta z = 0.9134$ nm. The accuracy of the angle mosaic errors is less than 0.2 μrad, and for the position mosaic errors it is less than 9 nm. This method simplifies the complex structure of the optical path and at the same time ensures measurement accuracy.

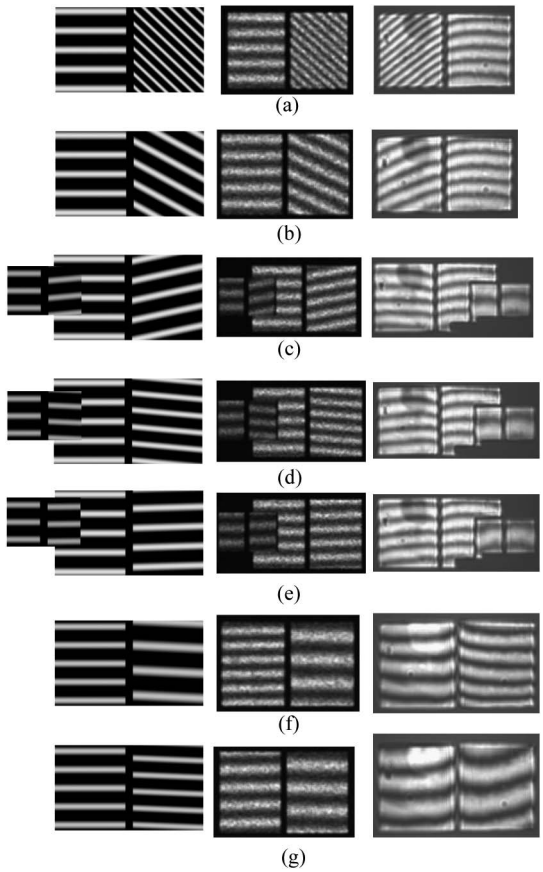

Fig. 8. Interference fringes of mosaic errors on the zero order and first order. (a) $\Delta\theta_x = 12.263\ \mu\text{rad}$, $\Delta\theta_y = 28.984\ \mu\text{rad}$, $\Delta z = -799.28$ nm; (b) $\Delta\theta_x = 1.833\ \mu\text{rad}$, $\Delta\theta_y = 10.035\ \mu\text{rad}$, $\Delta z = -305.16$ nm; (c) $\Delta\theta_x = -0.38062\ \mu\text{rad}$, $\Delta\theta_y = -4.1211\ \mu\text{rad}$, $\Delta z = 216.55$ nm; (d) $\Delta\theta_x = 3.5194\ \mu\text{rad}$, $\Delta\theta_y = 2.0671\ \mu\text{rad}$, $\Delta z = -130.15$ nm; (e) $\Delta\theta_x = -0.25578\ \mu\text{rad}$, $\Delta\theta_y = -0.53014\ \mu\text{rad}$, $\Delta z = -47.633$ nm; (f) $\Delta\theta_x = 0.9853\ \mu\text{rad}$, $\Delta\theta_y = -0.6258\ \mu\text{rad}$, $\Delta\theta_z = -48.5269\ \mu\text{rad}$, $\Delta x = 3.001$ mm, $\Delta z = -56.2356$ nm; and (g) $\Delta\theta_x = -0.6115\ \mu\text{rad}$, $\Delta\theta_y = -0.9587\ \mu\text{rad}$, $\Delta\theta_z = 18.3\ \mu\text{rad}$, $\Delta x = 3.000047$ mm, $\Delta z = -30.2$ nm.

5. CONCLUSION

In conclusion, a method to make perfect mosaic gratings in a single-interferometer system by adopting a small-aperture phase difference reference window is proposed and demonstrated. The reference window is achieved by adding a small-aperture prism; therefore, the incident light on the mosaic gratings contains two angles of incidence: one is the original beam without passing through the prism, and another is the small-aperture beam passing through the prism. For the reason that the same longitudinal mosaic error causes different optical

path differences between the original beam and small-aperture beam, the uncertainty of the longitudinal mosaic error can be eliminated on the zero order in the interferometer. The non-coplanar mosaic errors are eliminated combined with the reference window. Without the effect of the longitudinal mosaic error, the coplanar mosaic errors can be eliminated on the diffraction order.

The mathematical model of optical path difference between mosaic gratings for non-coplanar and coplanar mosaic errors is established. Different optical path differences of the original beam and the small-aperture beam are calculated, respectively, and the same fringes discontinuing for the original beam and the reference window interference fringes are served as criterion for longitudinal mosaic error alignment. When the alignment range of the longitudinal mosaic error is less than the specific value and there are no fringes discontinuing, the longitudinal mosaic error is equal to zero. The specific parameters are designed and the experimental optical path is set up. The experimental results are in agreement with simulation results which verify the correction of the method. The accuracy of the angle mosaic error is less than 0.2 μrad, and the position mosaic error is less than 9 nm. Our method reduces the complexity of optical path structure and removes five mosaic errors by using a single interferometer.

Funding. Key Scientific Instruments (ZDYZ2008-1); National Key Basic Research Program of China (2014CB049500); National Natural Science Foundation of China (NSFC) (61505204).

REFERENCES

1. N. Bonod and J. Neauport, "Diffraction gratings: from principles to applications in high-intensity lasers," Adv. Opt. Photon. **8**, 156–199 (2016).
2. M. P. Wood and J. E. Lawler, "Aberration-corrected echelle spectrometer for measuring ultraviolet branching fractions of iron-group ions," Appl. Opt. **51**, 8407–8412 (2012).
3. J. S. Pazder, S. Roberts, R. Abraham, A. Anthony, M. Fletcher, T. Hardy, D. Loop, and S. Sun, "WFOS: a wide field optical spectrograph for the thirty meter telescope," Proc. SPIE **6269**, 62691X (2006).
4. G. De Marchi, M. B. J. te Plate, S. M. Brikmann, T. Boker, P. Ferruit, G. Giardino, P. Jakobsen, M. Sirianni, J.-C. Salvignol, X. Gnata, R. Barho, M. Kosse, P. Mosner, B. Dorner, G. Cresci, F. Rosales-Ortega, M. Stuhlinger, T. Gross, and T. Leikert, "Calibrating the position of images and spectra in the NIRSpec instrument for the James Webb Space Telescope," Proc. SPIE **8150**, 81500C (2011).
5. R. G. Tull, "High-resolution fiber-coupled spectrograph of the Hobby-Eberly Telescope," in *Astronomical Telescopes and Instrumentation* (International Society for Optics and Photonics, 1998), pp. 387–398.
6. J. Qiao, A. W. Schmid, L. J. Waxer, T. Nguyen, J. Bunkenburg, C. Kingsley, A. Kozlov, and D. Weiner, "*In situ* detection and analysis of laser-induced damage on a 1.5-m multilayer-dielectric grating compressor for high-energy, petawatt-class laser systems," Opt. Express **18**, 10423–10431 (2010).
7. X. Wang, X. Wei, Y. Hu, X. Zeng, Y. Zuo, X. Hao, K. Zhou, N. Xie, and Y. Zhang, "Chirped-pulse amplification system based on chirp reversal and near-field spatial reversal with common tiled grating pair as stretcher and compressor," Appl. Opt. **51**, 5627–5632 (2012).
8. Z. Li, S. Li, C. Wang, Y. Xu, F. Wu, Y. Li, and Y. Leng, "Stable and near Fourier-transform-limit 30 fs pulse compression with a tiled grating compressor scheme," Opt. Express **23**, 33386–33395 (2015).
9. Z. Li, T. Wang, G. Xu, D. Li, J. Yu, W. Ma, J. Zhu, L. Chen, and Y. Dai, "Research on potential problems of object image grating self-tiling for applications in large aperture optical systems," Appl. Opt. **52**, 718–725 (2013).
10. M. J. Algots, R. A. Bergstedt, W. N. Partlo, G. E. Rylov, and R. L. Sandstrom, "Line narrowing module," U.S. patent 8126027 B2[P] (February 28, 2012).
11. Z. Tao, J. Cui, and J. Tan, "Simultaneous multi-channel absolute position alignment by multi-order grating interferometry," Opt. Express **24**, 802–816 (2016).
12. J. Hoose, E. Loewen, R. Wiley, T. Bzasiak, S. Zheleznyak, and T. Sroda, "Grand gratings: bigger is better, thanks to mosaic technology-today's larger telescopes' unprecedented challenge," Photon. Spectra **29**, 118–136 (1995).
13. T. Blasiak and S. Zheleznyak, "History and construction of large mosaic diffraction gratings," in *International Symposium on Optical Science and Technology* (International Society for Optics and Photonics, 2002), pp. 370–377.
14. T. Harimoto, "Far-field pattern analysis for an array grating compressor," Jpn. J. Appl. Phys. **43**, 1362–1365 (2004).
15. L. Zeng and L. Li, "Method of making mosaic gratings by using a two-color heterodyne interferometer containing a reference grating," Opt. Lett. **31**, 152–154 (2006).
16. J. Qiao, A. Kalb, T. Nguyen, J. Bunkenburg, D. Canning, and J. Kelly, "Demonstration of large-aperture tiled-grating compressors for high-energy, petawatt-class, chirped-pulse amplification systems," Opt. Lett. **33**, 1684–1686 (2008).
17. J. Qiao, A. Kalb, T. Nguyen, D. Canning, and J. Price, "Development and operation of large-aperture tiled-grating compressors for high-energy, petawatt-class laser systems," in *Frontiers in Optics 2010/Laser Science XXVI* (Optical Society of America, 2010), paper FTuR5.
18. Y. Hu and L. Zeng, "Grating mosaic based on image processing of far-field diffraction intensity patterns in two wavelengths," Appl. Opt. **46**, 7018–7025 (2007).
19. Y. Hu, L. Zeng, and L. Li, "Method to mosaic gratings that relies on analysis of far-field intensity patterns in two wavelengths," Opt. Commun. **269**, 285–290 (2007).
20. J. Qiao, A. Kalb, M. Guardalben, G. King, D. Canning, and J. Kelly, "Large-aperture grating tiling by interferometry for petawatt chirped-pulse-amplification systems," Opt. Express **15**, 9562–9574 (2007).

159.226.165.13 {ts '2017-06-22 23:07:09'}